Ann. Geophys., 27, 3677–3690, 2009
www.ann-geophys.net/27/3677/2009/

Annales Geophysicae

On acceleration of <1 MeV/n He ions in the corotating compression regions near 1 AU: STEREO observations

R. Bučík[1,2], **U. Mall**[1], **A. Korth**[1], **and G. M. Mason**[3]

[1]Max-Planck-Institut für Sonnensystemforschung, 37191 Katlenburg-Lindau, Germany
[2]Institute of Experimental Physics, 04001 Košice, Slovakia
[3]The Johns Hopkins University Applied Physics Laboratory, Laurel, MD 20723, USA

Received: 22 June 2009 – Revised: 4 September 2009 – Accepted: 9 September 2009 – Published: 30 September 2009

Abstract. Observations of multi-MeV corotating interaction region (CIR) ions are in general consistent with models of CIR shock acceleration and transport. The presence of suprathermal particles near 1 AU in unshocked compression regions is not adequately explained. Nonetheless, more recent works demonstrate that unshocked compression regions associated with CIRs near 1 AU could energize particles. In the energy range from ∼0.1 to ∼1 MeV/n we investigate CIR events observed in 2007–2008 by the STEREO A and B spacecraft. We treat the predictions of compression acceleration by comparing the observed ion intensities with the model parameters. These observations show that the ion intensity in CIR events with in-situ reverse shock is well organized by the parameters which characterize the compression region itself, like compression width, solar wind speed gradients and the total pressure. In turn, for CIR events with the absence of the shocks the model predictions are not fulfilled.

Keywords. Interplanetary physics (Energetic particles; Solar wind plasma) – Space plasma physics (Charged particle motion and acceleration)

1 Introduction

Recent works (e.g., Mason, 2000; Chotoo et al., 2000) pointed out that measurements of corotating interaction region (CIR) suprathermal ions at 1 AU from the Sun are inconsistent with the standard picture associated with multi-MeV particles where the acceleration occurs by forward and reverse shocks bounding the CIR at several AU and the particles propagate into the inner heliosphere (Barnes and Simpson, 1976; Christon and Simpson, 1979). The peak intensities at the low energies are observed within the CIR at places that are not magnetically connected to the shock (Richardson and Zwickl, 1984). Moreover, a turnover of the spectra below a few 10s of keV/n, as predicted by CIR models, is not observed (Mason et al., 1997, 2008a). These observation features suggest that the ions are accelerated more locally. Usually, there were no shocks observed at ∼1 AU and therefore, other non-shock energizing mechanisms have been suggested. It may be a stochastic mechanism related to increased turbulence levels in the CIRs, which accelerate particles by scattering from Alfvén and magnetosonic waves or by transit-time damping (Richardson, 1985; Schwadron et al., 1996; Fisk and Gloeckler, 2006), or an acceleration in the compressed region of the solar wind (Giacalone and Jokipii, 1997; Giacalone et al., 2002).

Giacalone et al. (2002) showed that compression regions associated with the CIRs at 1 AU with the absence of shocks can accelerate particles to high energies. The mechanism is similar to diffusive shock acceleration, in that the energy gain arises from scattering between converging scattering centers. These authors pointed out that particles are efficiently accelerated because the total compression is very large. They found that the efficiency of the acceleration depends on the compression width – the thinner compression produces the higher intensity. The efficiency also depends on the particle mean free path – it must be larger compared to the width of the compression region but smaller than about 1 AU. In this case the particles can cross the accelerating region several times, which is equivalent to the condition in shock acceleration. The model predicts the upper limit for the compression width given by the Eq. (2) in Giacalone et al. (2002). At a fixed heliocentric distance this limit is given by relative change in the flow speed – the higher maximum width corresponds to the higher relative change in the flow speed. For example, if the solar wind speed changes from 300 to 700 km/s across the compression region at 1 AU, the compression width must be below ∼0.3 AU for acceleration to

Correspondence to: R. Bučík
(bucik@mps.mpg.de)

Table 1. Time intervals and type of edges of CIRs included in this study.

CIR	STEREO-A		STEREO-B	
#	Start date...Stop date	Edges	Start date...Stop date	Edges
2007				
01	02–25/21:30...02–28/11:00 c	| |		
02	03–11/05:08...03–13/03:40	| \	03–11/10:40...03–13/08:10	| \
03	03–31/20:00...04–02/10:00	| |	03–31/23:15...04–02/13:30	| |
04	04–08/18:20...04–12/06:00 c	| \	04–09/02:00...04–12/09:50 c	| \
05	05–07/08:10...05–08/20:30	| |	05–07/09:50...05–08/14:00	| |
06	05–18/07:00...05–19/05:40	/ |	05–17/21:30...05–19/08:00	| \
07	05–31/23:50...06–04/21:30 c	/ \	06–01/02:30...06–04/04:00 c	| \
08	07–11/03:40...07–11/20:23	| |	07–10/15:40...07–11/07:40	| |
09			07–19/23:20...07–20/18:10	| |
10			08–06/02:50...08–07/02:00	| \
11	08–25/20:30...08–27/23:00	| \		
12	09–21/14:20...09–23/11:20 c	| |	09–19/18:15...09–22/00:50 c	| |
13	09–28/18:30...09–30/11:10	| |	09–26/16:10...09–29/07:40 c	| |
14	10–25/19:30...10–27/13:00	| \	10–23/10:20...10–25/10:50 c	| |
15	11–14/01:30...11–15/15:50	/ \		
16	11–20/21:10...11–21/12:40	| |	11–19/14:00...11–20/23:00	| \
17	12–12/07:50...12–13/04:10	| |	12–08/22:50...12–10/11:20	| |
18			12–16/00:30...12–19/06:10 c	| |
2008				
19	01–06/17:00...01–08/01:40	| |	01–03/09:10...01–04/18:30	| |
20	02–02/09:20...02–05/00:50 c	| |	01–29/22:20...01–31/17:30	| \
21	02–11/11:30...02–13/04:30	| |	02–09/04:40...02–09/18:40	| |
22	02–29/23:00...03–02/06:00	| |	02–26/21:30...02–28/09:25	| |
23	03–08/18:17...03–09/19:50	| |		
24	03–28/01:40...03–29/18:10	| |	03–23/08:50...03–25/16:00 c	/ \
25			04–01/23:20...04–04/07:41 c	| |
26	04–24/13:10...04–25/03:30	| |		
27	06–16/10:20...06–17/16:10	| |		
28			07–19/07:30...07–21/10:20 c	| |
29	08–08/05:20...08–11/10:50 c	| \	08–06/21:00...08–08/21:10	| |
30			08–16/00:25...08–16/12:30	| |
31			09–01/05:20...09–03/17:30 c	| |
32			09–28/02:40...09–29/13:08	| |

occur. Note, this type of acceleration was used in the study of propagation and acceleration of solar energetic particles (SEPs) inside CIRs (Kocharov et al., 2003), and also applied to the magnetosphere (Zhang, 2006).

The authors of this new model reported that the predicted hydrogen and helium energy spectra are remarkably similar to the observations but no extensive comparison considering many events has been performed. In this work we use observations of suprathermal helium ions by STEREO at ∼1 AU during the 2007 and 2008 solar minimum period. The purpose of this work is to examine the compression acceleration mechanism in CIRs. We start with the list of the compression regions analyzed in this survey in Sect. 2.1. In Sect. 2.2 we present observations of all the analyzed events and determine the CIR boundaries. The complex events of this survey are treated in Sect. 2.3. In Sects. 2.4 and 2.5 we investigate the relation between the ion intensity and the thickness of the compression region, total pressure and solar wind speed gradients. Finally, in Sects. 3 and 4, we discuss and summarize the results.

2 Observations

The measurements presented here were made with the Suprathermal Ion Telescope (SIT) (Mason et al., 2008b) onboard the STEREO spacecraft, A and B (Kaiser et al., 2008), launched in October 2006. Both STEREO spacecraft are placed on heliocentric orbit, STEREO-A preceding the Earth and STEREO-B trailing behind. For the period analyzed here, February 2007–September 2008, the heliocentric distance varied from 0.96 to 0.97 AU for STEREO-A and 1.00−1.09 AU for STEREO-B. The SIT instrument is

a time-of-flight mass spectrometer which measures H to Fe ions from 20 keV/n to several MeV/n. In our study we also make use of energetic hydrogen ion measurements, made by the LET instrument (Mewaldt et al., 2008), solar wind measurements made by the PLASTIC instrument (Galvin et al., 2008) and magnetic field measurements obtained by the magnetometer on STEREO (Acuña et al., 2008).

2.1 Event selection

Table 1 lists CIRs investigated in this paper. We limited our study on interval February 2007–September 2008, where the solar wind plasma data were available. The leftmost column is the CIR number. Columns 2, and 4 list the start and end times at STEREO-A and B in the format Month-Day/HH:MM. The letter c marks CIR with a compound solar wind stream. The character of the CIR boundaries (determined by the total pressure P) is shown in Columns 3 and 5. The vertical short lines indicate well-defined boundaries. Red color marks the edges bounded by the shocks. The slant lines indicate inaccurately defined CIR edges. The corresponding CIR ion events are included in the survey of Mason et al. (2009). The authors selected only those events where the hourly average intensity of 189 keV/n He exceeds 10 particles/cm^2 s sr MeV/n. We apply the same criterion for selection of the CIRs. Note that for CIR 01 on STEREO-B and CIRs 18 and 32 on STEREO-A there were no solar wind plasma data available. Other missing dates in Table 1 mean that ion intensity was below the selection threshold. Thus, we have 24 CIR events observed by STEREO-A and 26 events by STEREO-B. From those events, equally, 8 CIRs on STEREO-A and 8 CIRs on STEREO-B were accompanied by in-situ reverse shocks. The shock locations were identified using the list compiled by the STEREO magnetometer team at the University of California Los Angeles, based on plasma and magnetic field data (http://www-ssc.igpp.ucla.edu/forms/stereo/stereo_level_3.html). The list of the interplanetary coronal mass ejections (ICMEs) observed by STEREO, provided by the same team, is also used in this paper.

The predictions of the acceleration model can be compared with observations on the assumption that the seed population is constant. During the solar minimum the variations in the seed intensity due to temporal effects are probably negligible as long as the occurrence of the solar transients is very low. The low rate of the solar transients during the investigated period was reported by Gómez-Herrero et al. (2009). The 24 May 2007 CIR event was a priori excluded from the analysis. For this event the boundaries of the CIR were not clear due to preceding ICME. In addition, the CIR associated ion intensity was affected by the 23 May 2007 SEP event (Bučík et al., 2009). We searched for other STEREO SEP and CIR events coincidences. The high energy 6−10 MeV proton observations from the LET instrument indicate two other weak SEP events with onsets on 5 April and 26 April 2008, observed by STEREO-A and B, respectively. No one preceded or occurred during the CIR event in this survey. It is generally accepted that He^+ pick-up ions could be an important seed population for acceleration in CIRs. The spatial distribution of such ions in the inner heliosphere is not uniform due to the focusing effect of the gravitational field of the Sun (Möbius et al., 1985). However, the variability at suprathermal energies is not clear. Klecker et al. (2001) and Möbius et al. (2002) found little evidence to support a suggestion of Kallenbach et al. (2000) that the He^+/He^{2+} ratio may reflect the spatial variation of the pick-up He source. Therefore, in this survey we consider all CIR events when STEREO traversed the helium focusing cone, which occurred on 10–30 November 2007 by STEREO-A and between 9 December 2007 and 18 January 2008 by STEREO-B (B. Klecker, private communication, 2009).

2.2 CIR boundaries

The leading edge (LE) of the interaction region is characterized by an increase in plasma density, temperature and magnetic field intensity and the trailing edge (TE) by a decrease in these quantities (Smith and Wolfe, 1979). The solar wind speed increases at both edges. So long as there is no shock formed at these boundaries the edges of the CIR represent continuous transition zones (Belcher and Davis, 1971) and there is some uncertainty in the location of the boundaries (Richardson and Zwickl, 1984). The front and rear of the interaction region are also characterized by an abrupt increase and decrease in total pressure, and the high pressure occurs generally in the rising part of the speed profile (Burlaga, 1995).

Figures 1 and 2 display the CIR events listed in Table 1 at STEREO-A and B, respectively. Each subfigure contains three panels. The top panels present hourly averaged He ion intensities (particles/cm^2 s sr MeV/n) in seven energy channels between 0.136 and 1.088 MeV/n. The middle panels show 10 min averages of the solar wind speed V and the bottom panels the total pressure P, which is given by the sum of the plasma and magnetic field pressure, i.e. $P=2n_pkT_p+B^2/2\mu_0$, where n_p and T_p are the proton density and temperature, respectively, and B is the magnetic field magnitude. Pairs of vertical solid lines mark the CIR boundaries. We use total pressure in identifying the compression regions. Earlier works (Gosling and Pizzo, 1999; Jian et al., 2006) demonstrated that total pressure has much simpler signatures than the constituent components. By visual inspection of the pressure profile we selected the CIR boundaries at times when 10 min pressure data showed an abrupt change. Except for CIRs bounded by forward (reverse) shock we found few other CIRs with well-defined boundaries where total pressure shows rather a jump-like increase (decrease) than the continuous changes. The type of the CIR edges is shown in Table 1. For the visibility of the CIR boundaries the limited range of the total pressure (below 0.2 nPa) is shown in

Figs. 1–2. We found that for all events where CIR boundaries were well defined the total pressure exceeded 0.05 nPa. Note, in background solar wind, P is typically 0.02−0.03 nPa (Jian et al., 2006). Thus, for CIRs with continuous changes in the pressure, the compression region boundaries were selected at times when the total pressure reaches 0.05 nPa or descends below this value. But some CIRs showed quite complex pressure profile, varying around the selected pressure threshold. In such cases we additionally required an increase in the solar wind speed. It concerns the definition of TEs for CIRs 02A, 02B and 15A. The highly variable pressure during CIR 02B is related to STEREO-B's pass near the magnetospheric tail (at geocentric distance of 400 Re) in March 2007.

The vertical dashed lines in Figs. 1–2 mark the location of the reverse shock inside the CIR 15A, 06B, 10B and 13B. The CIR 13B is accompanied by two reverse shocks, one bounding CIR TE and other located within CIR. The reverse shocks reported for the events 15A, 06B and 10B are probably not bounding the compression regions itself. The reverse shock in 06B occurred in the middle of the enhanced pressure. This shock has clear indication from the magnetic field data but not from the plasma data. Concerning the event 15A the reverse shock occurred during the rising part of the solar wind speed profile and the pressure was still enhanced after the shock passage. For the event 10B we observe a more abrupt change in P at the actual location of the trailing boundary than at the position of the reverse shock. However, no big departure from the reverse shock position is seen. For both 15A and 10B the reverse shock is not clear in magnetic field data.

Figures 1–2 demonstrate that total pressure shows a very complex time profile in CIRs. The solar wind speed shape is somewhat simpler. There are CIRs in the investigated period where the rising part of the solar wind speed profile contains one or more anomalous peaks. In accordance with Burlaga (1995), if such velocity maximum corresponds to the distinct pressure peak, then the high-speed solar wind stream is identified as a compound stream. The CIRs with compound streams, indicated in Table 1, are treated separately. Other CIRs in this survey have solar wind streams classed as simple streams. In the next sections some of the compound-stream CIRs are decomposed and analyzed in the CIR group with the simple streams.

Sanderson et al. (1998) found that the tilt of the current sheet and the position of the spacecraft relative to the Sun's equator play a role in determining the pattern of the high-speed streams and compression regions seen at 1 AU, which influence the intensity and occurrence of the CIR-related particles. Throughout the February 2007 and September 2008 the computed tilt angle (http://wso.stanford.edu/Tilts.html) shows an almost flat time profile varying between 26° and 36°. Since the change is quite small we suppose this variance could not considerably affect the location of the compression region boundaries. During this period STEREO traversed the range of heliographic latitudes from −7° to 7°. In the model of Giacalone et al. (2002) the energetic particles are accelerated locally within the transition region from slow to fast solar wind. In respect of this we may assume that the particle intensity observed at the particular latitude is related to the characteristics of the compression region measured around the same position.

In some events the He intensity remains high, long after the CIR period has passed. For example the events A05 and A19 last about one third of the solar rotation period. Both A05 and A19 were accompanied by in-situ reverse shock. Outside of the compression region, the event A05 is characterized by a gradual softening of the helium energy spectra (deduced from the distances between intensity lines in different energy channels), whereas in the event A19 the energy spectrum hardens with time. The hardening of the energy spectra is believed to be due to a propagation effect (e.g., Mason et al., 1999). The connection to the distant source in this case persisted for a long time. The time profile of the He intensity in the event A05 is much more variable compared to the A19. One order of magnitude intensity increase in the middle of the intensity time profile (11 May 2007) occurred during the small, ∼60 km/s, increase in the solar wind speed. This speed rise was not accompanied by formation of the compression region. The episodes of the intensity decreases followed by an increase a few hours later appear to be due to changes in connection to the CIR caused by associated solar wind speed changes (Mason et al., 2009). The intensity increase on 29 March 2008 after passage of the CIR 24B is probably associated with the next event (CIR 25B) forward compression as suggested by the SEP-like He/H abundance ratios (not shown). Note the He/H ratio at corotating forward shocks is lower than that at the reverse shocks (Barnes and Simpson, 1976). The intense enhancement after passage of the CIR06 was associated with the CIR event on 24 May 2007.

2.3 Complex CIRs

Figures 1–2 show that three compound CIRs, namely 01A, 24B and 28B, have two stream components clearly distinguishable and the predecessor streams are not accompanied by the ion intensity enhancements. These events are also treated as simple stream events with the second i.e. major solar wind stream component. The CIR 29A is similar to the three previous events but with no clear leading boundary of the second compression zone. Therefore this event is left for the group of CIRs with compound streams.

The compound stream of the CIR 18B apparently consists of two components. It is likely that the major ion intensity enhancement is associated with only the first stream component. There is no enhancement during the high-speed solar wind of the second component and within second compression zone the ion intensity continues to decrease with the small peak at the leading edge of the second stream. The

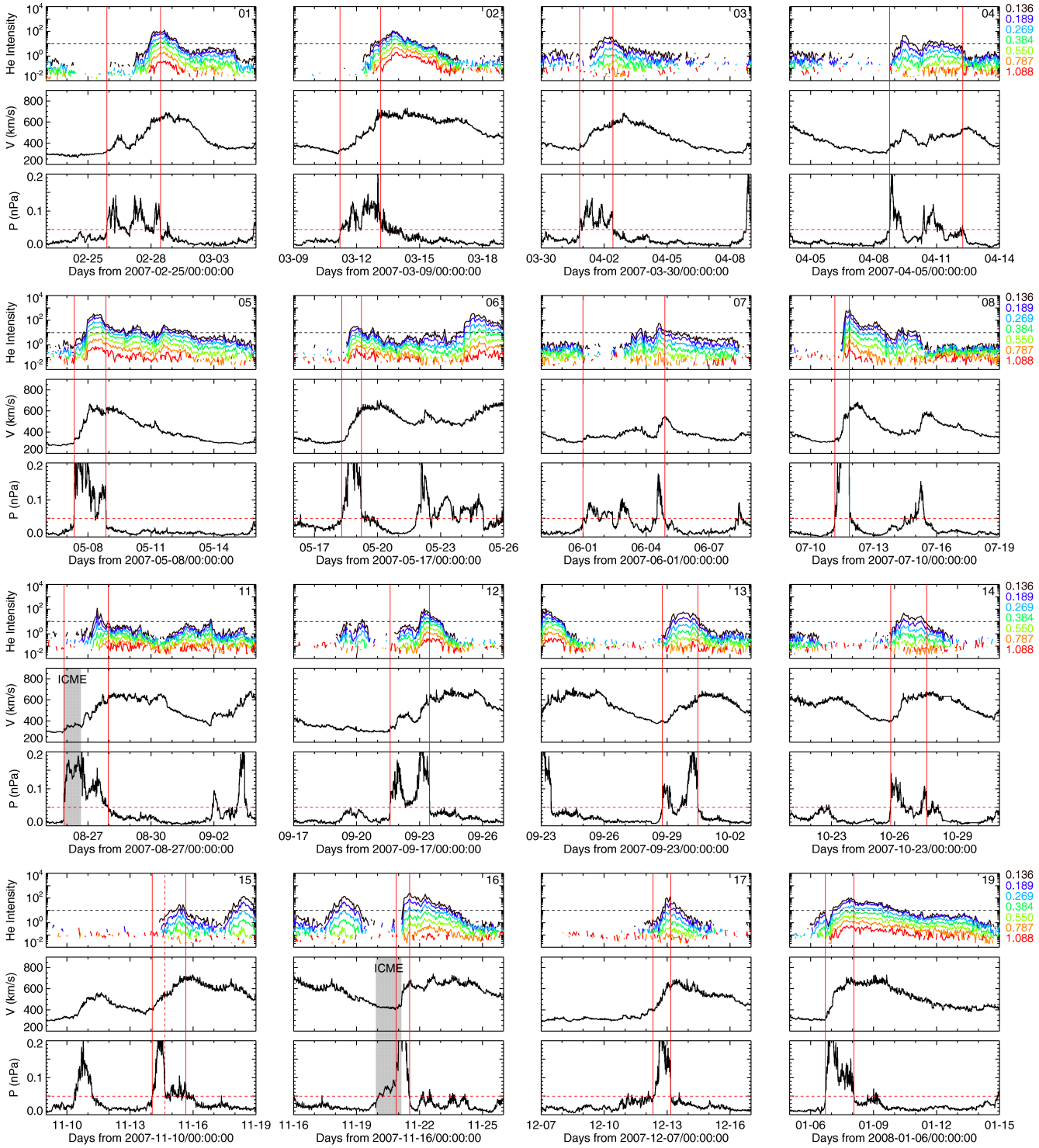

Fig. 1. STEREO-A measurements associated with the CIRs listed in Table 1. There is one subfigure for each event. The event number is displayed in the upper right corner. The subfigure contains three panels. Top panel: hourly averaged He ion intensities in seven energy channels between 0.136 and 1.088 MeV/n. Middle panel: 10 min averages of the solar wind speed V. Bottom panel: the total pressure P. Pairs of vertical solid lines mark CIR boundaries corresponding to the times in Table 1. The vertical dashed line marks location of the reverse shock inside the CIR. The gray shaded regions mark the time intervals of the ICMEs.

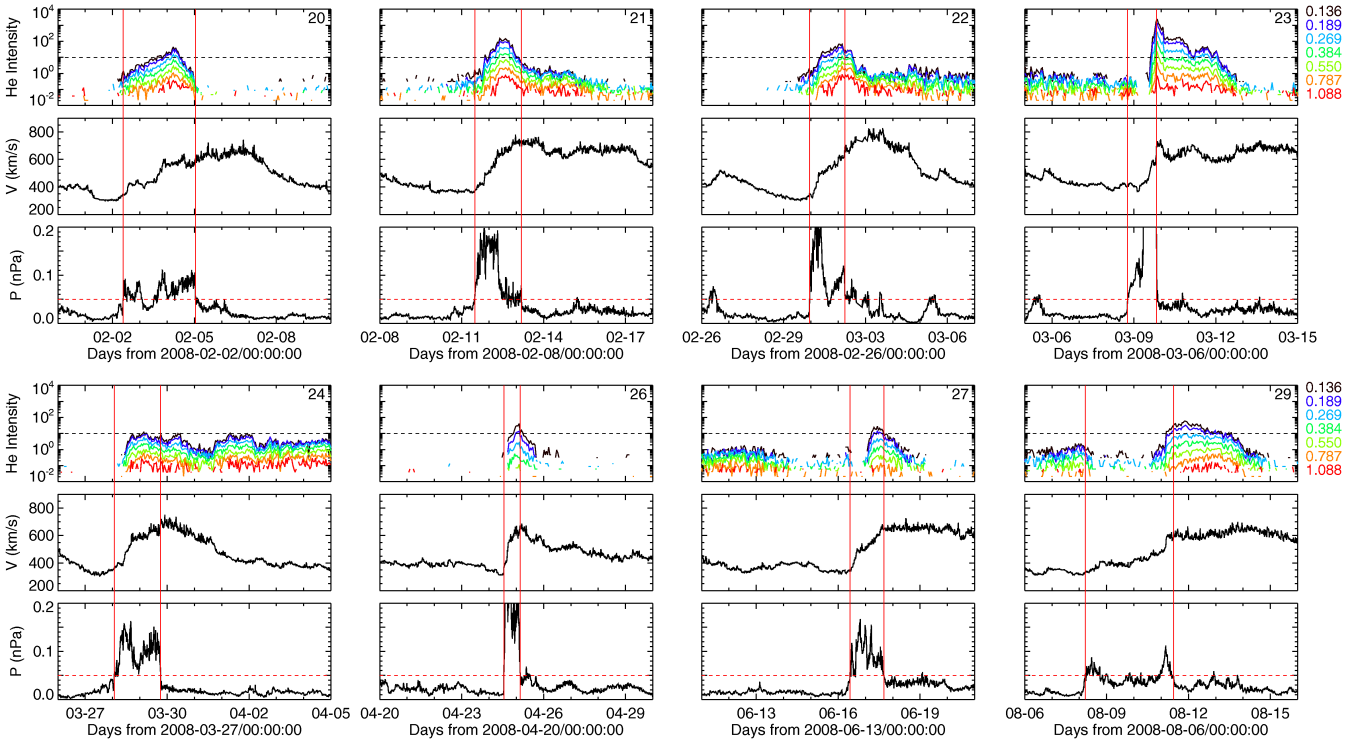

Fig. 1. Continued.

predecessor compression zone of this event is also analyzed in the group of events with simple streams.

The CIRs 04A, 04B, 12B, and 13B consist of two major stream components. The energetic particle observations also show two corresponding intensity enhancements. Figures 1–2 show that the second ion enhancement is only confined to the rising part of the second stream component or to the corresponding compression region. When the solar wind speed stops rising the ion intensity suddenly decreases. The similar feature was observed for event 18B. It is likely that the second stream causes only an additional intensity increase and does not create an autonomous event. It is also supported by fact that the total pressure is much higher in the predecessor compression component. As a result the boundary of the second compression is poorly defined. Therefore, as a simple stream event, we consider only the initial stream component. Mason et al. (2009) explained similar dropouts in ion intensity in terms of changing the magnetic connection to the source region. Although the online catalog does not list the reverse shock bounding the TE of the first compression component in the event 04B, the peaked He ion intensity and the jump decrease in the total pressure on 9 April 2007 suggests the local reverse shock as an ion source. The ion enhancement in the event 31B is also confined to the complex compression region which consists of three major pressure peaks. This event with the first compression and corresponding ion enhancement is considered for the group of the simple stream events. The online list again does not indicate the in-situ reverse shock, but similar to the event 04B, peaked ion intensity and an abrupt decrease in total pressure on 3 September 2008 suggests the shock related ion increase.

The event 12A also consists of two stream components and the corresponding two energetic particle increases. The first increase was below the selection threshold. The second ion enhancement is likely not only confined to the time duration of the corresponding compression region but continues in the high-speed solar wind. However, we do not detach the second stream component since the leading boundary is not very clear.

The event 20A is characterized by a single ion enhancement with the rise and decay confined to the duration of the compression region. The compression region consists of two parts and due to single ion enhancement the event is not divided into the two components. The event 25B is likely composed of three streams. The weak ion enhancement at the beginning of the compression zone is associated with the previous event. The ion enhancement started to increase with the onset of the second stream. The event is again not separated into the smaller parts, due to the complex ion intensity enhancements.

The compression regions 07A and 07B likely consist of three components. The energetic particle increase starts with the second solar wind stream and continues to increase with the onset of the third stream. These two events look like

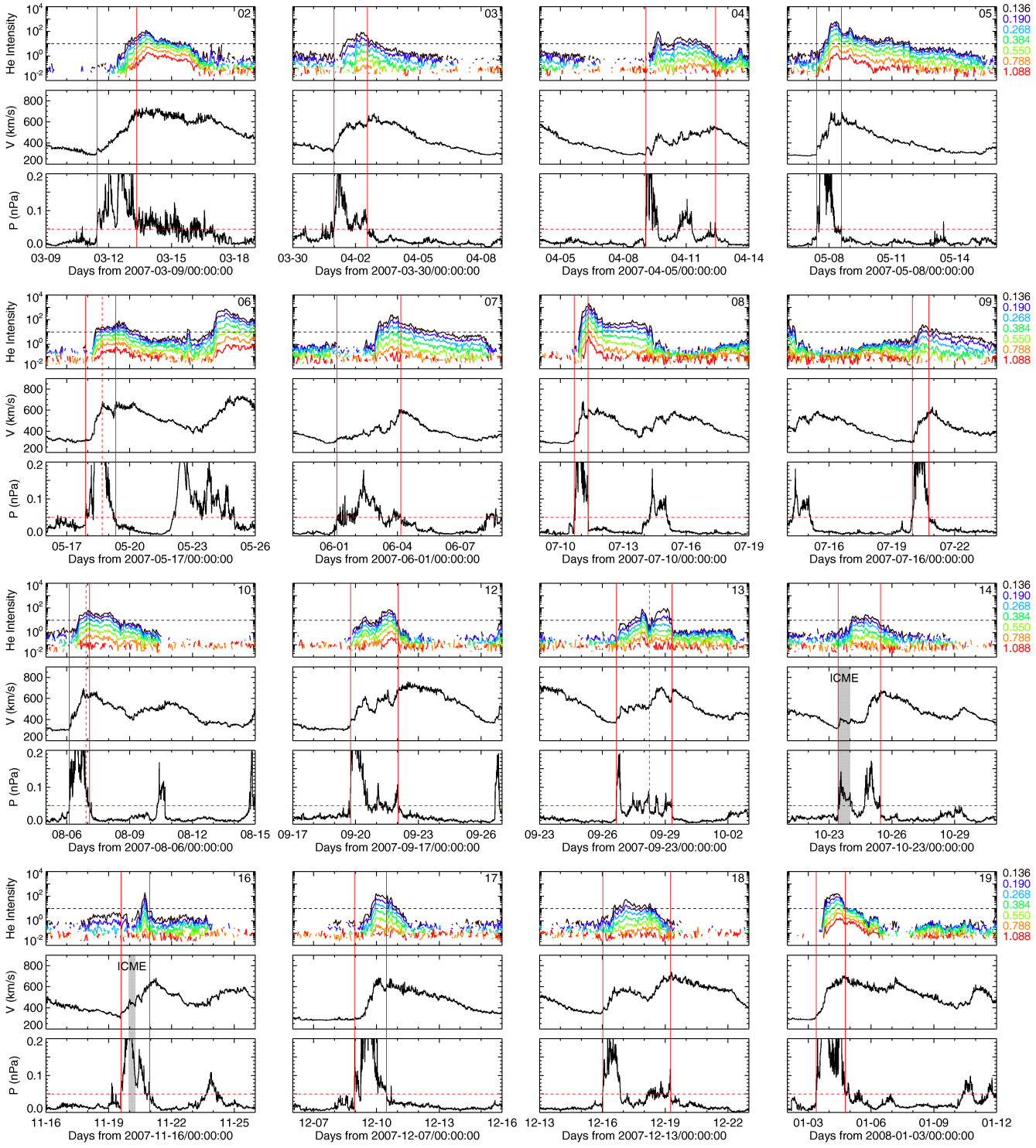

Fig. 2. Same as Fig. 1 but for STEREO-B.

autonomous events, with ion intensity varying with solar wind speed. The events are not decomposed.

The event 14B is a complex corotating event with an ICME which occurred during the first solar wind stream component, as indicated in the online catalog. This stream

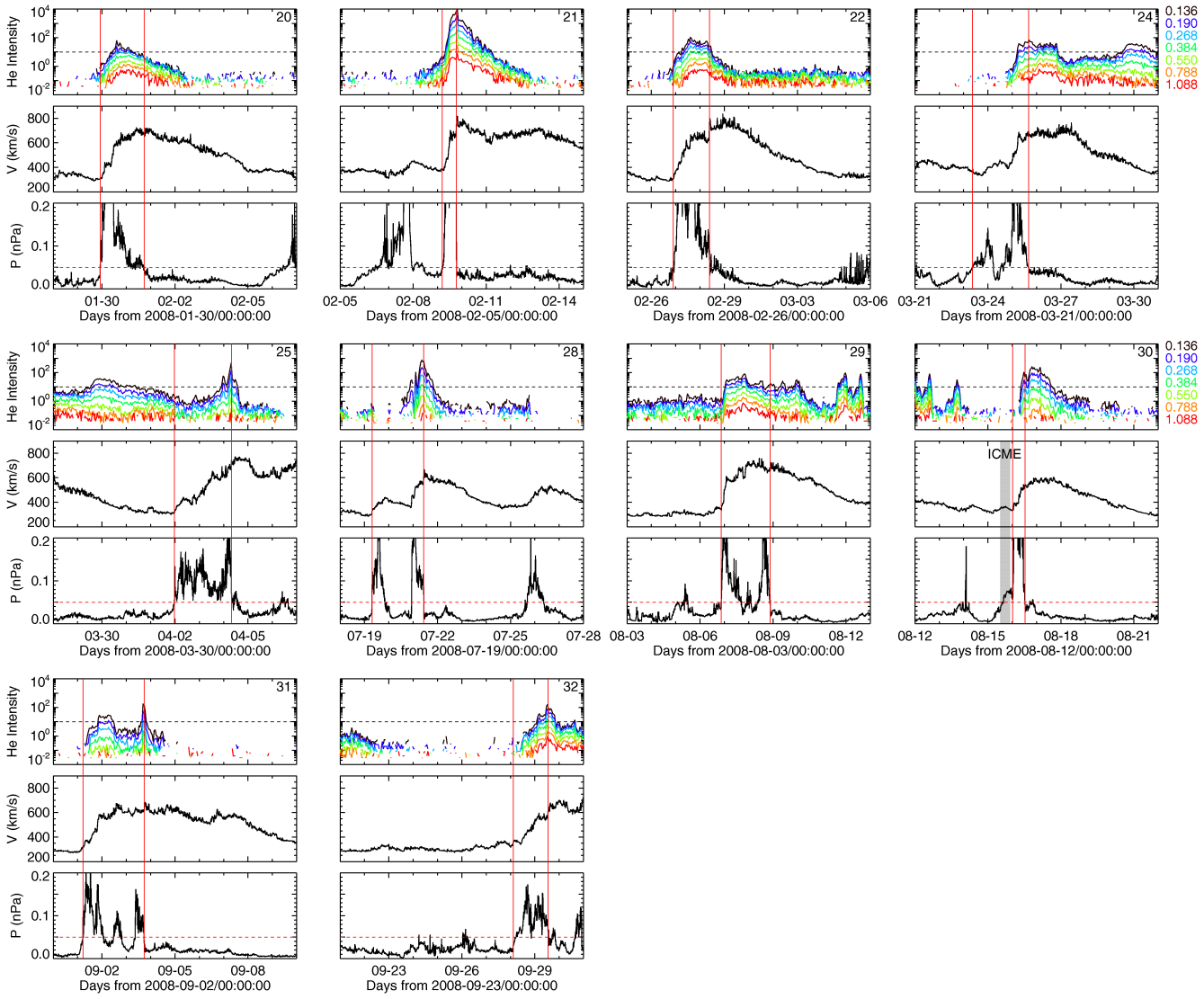

Fig. 2. Continued.

is quite slow with a speed around 400 km/s. The ion increase began during the valley between two distinct pressure peaks and weakly increased with the second high-speed (∼700 km/s) stream component. This event is also left in the group with compound streams.

2.4 Peak intensity vs. compression width

Figure 3 shows a 0.189 MeV/n He ion event-peak hourly average intensity vs. the compression width. The statistical errors in the He peak intensities are quite low and vary between 0.4 to 8.1% with the median value of 3.8%. All events are separated into five sets by peak pressure over the compression region. The events with simple streams are marked by triangles and the compound streams by circles. Upper panel shows CIRs with in-situ reverse shocks, and lower panel CIRs without in-situ reverse shocks. Although the highest peak intensity corresponds to the highest peak pressure (event 21B), there is no clear relationship between peak intensity and the peak pressure. In the next section we demonstrate that the events with the in-situ reverse shocks show better ordering with the total pressure. Figure 3 also shows that CIRs with the highest peak pressure (>400 pPa) have thinner compression region (<0.5 AU).

The thickness of the compression region along the given radius vector is given by the expression $W\Delta\phi/\Omega$, where W is a constant speed at which the compression moves radially outward in the inertial (not rotating) frame of reference, $\Delta\phi$ is an azimuthal width of the compression region, and Ω is the Sun rotation rate (Giacalone et al., 2002). We estimate the

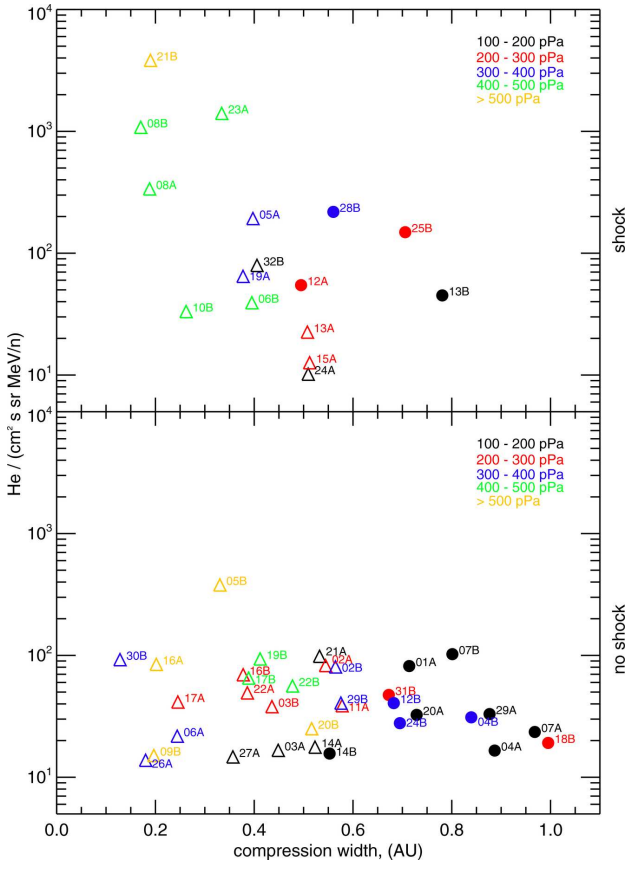

Fig. 3. Peak intensity for 0.189 MeV/n He vs. compression width. Upper panel: CIRs accompanied by in-situ reverse shocks. Lower panel: CIRs without in-situ reverse shocks. The events with simple streams are marked by triangles; compound streams are marked by circles. Different colors mark different peak pressure over the compression region.

width of the compression regions for CIRs in this survey by the above formula. The azimuthal width of the compression region was determined from the measured duration of the event. CIRs develop when the fast solar wind stream collides with the slow solar wind stream. Therefore, it is reasonable to assume that parameter W is somewhere between the fast and slow wind speed and may be represented by the velocity of the interface between two interacting streams. Siscoe (1976) pointed out that the two streams have about the same mass flux density and argued that the velocity of the stream interface would thus be close to the average of slow and fast wind speed. Following Siscoe (1976), we approximate the velocity W by the mean of maximum and minimum solar wind speed across the compression region. Observations in Figs. 1–2 indicate that the minimum and maximum speeds roughly correspond to the speeds of the slow and fast solar wind, respectively. Averaged over all 50 CIRs, the compression width is 0.50±0.03 AU and varies from 0.13 to 1.00 AU.

Table 2. Correlation between 0.189 MeV/n He ion peak intensity and compression width for CIRs with simple and compound streams.

	simple CIRs		compound CIRs	
	shock	no shock	shock	no shock
n	12	22	4	12
ρ	−0.76	0.09	−0.40	−0.27
p.100%	0.4	69.3	59.8	40.5

n – number of events, ρ – Spearman's correlation coefficient, p – two tailed probability value of a t-test

In survey of 365 CIRs, Jian et al. (2006) reported that the width of the CIRs varies from 0.06 to 1.24 AU, with a mean of 0.41±0.01 AU. The authors estimated the CIR size based on the measured duration and mean of maximum and minimum velocity inside the CIR.

We found that approximately 60% of the events were with suprathermal He peak intensity inside the compression region, 30% events peaked at the trailing boundary and only 10% events have an intensity peak outside the CIR. In the majority of the events there were no ions or its number was very low during the phase of the slow solar wind, closely preceding the compression region or at the leading boundary of the CIR. Here the ion intensity would be nominally associated with the distant or in-situ forward shock, respectively. Much lower intensities near the forward shock when compared with that found typically near the reverse shock were observed previously (e.g., Barnes and Simpson, 1976) and also predicted by the theory (Fisk and Lee, 1980).

Figure 3 (lower panel) shows that CIR 30B has the smallest compression width. For this event there were ICME adjacent to the front of the CIR and therefore, an interaction between traveling and corotating compression regions may occur. Event 16A is another example of the CIR event closely preceded by the ICME. Interestingly, the corresponding symbol in Fig. 3 is not far from the symbol for the event 30B. On S/C B the same ICME was found inside the CIR (16B). The figure shows event 16B is not moved to the low compression widths. Perhaps the presence of the ICME adjacent to the front of the CIR constricts the compression region but without a corresponding increase in ion intensity. Other events with ICME within the compression are 11A and 14B. Apparently, the width of these two CIRs is not reduced.

Table 2 shows correlation coefficient between 0.189 MeV/n He peak intensity and a compression width for CIRs with simple and compound streams. The correlations are shown separately for CIRs bounded by reverse shocks and for CIRs without in-situ reverse shocks. Already Fig. 3 has indicated that the peak intensity and the compression width are inversely correlated for events with in-situ reverse shock. Table 2 shows that there is no correlation between investigated quantities for simple-stream CIR events with

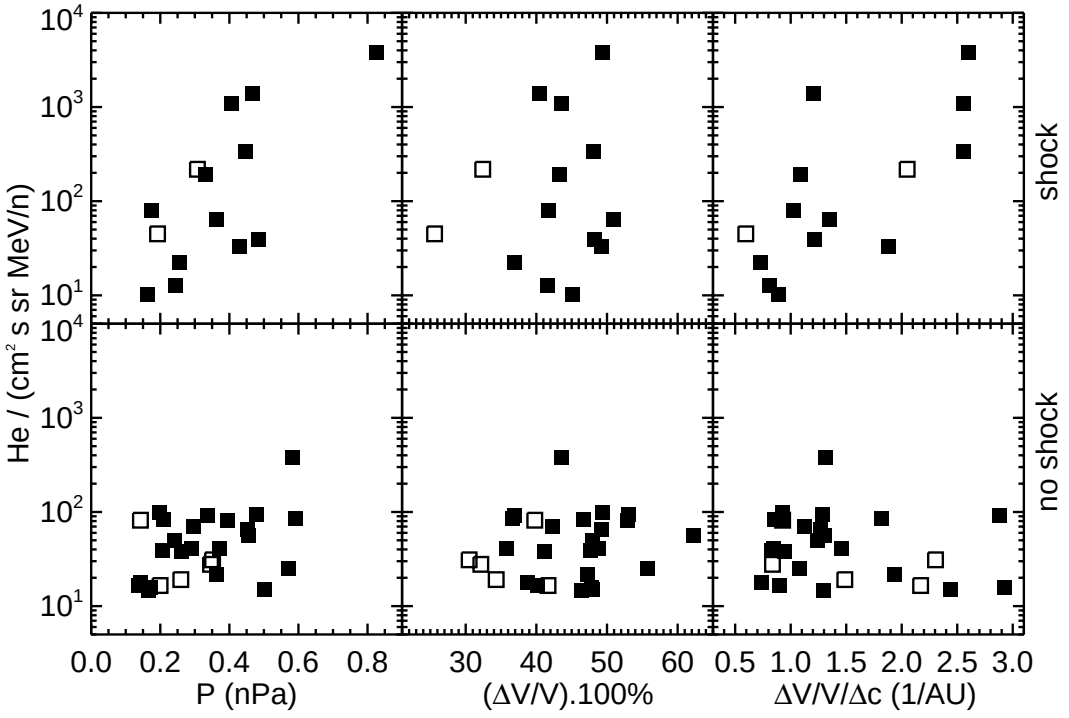

Fig. 4. Peak intensity for 0.189 MeV/n He vs. peak pressure (left panel), relative flow-speed change (middle panel) and relative flow-speed change per width of the compression region (right panel) for CIRs with simple streams. Upper panels: CIRs accompanied by reverse shocks. Lower panels: CIRs without in-situ reverse shocks. Open symbols indicate data added after decomposition of the events with compound streams.

Table 3. Correlations between 0.189 MeV/n He ion peak intensity and pressure peak P, relative change in the solar wind speed $\Delta V/V$ and relative change in the solar wind speed per compression width $\Delta V/V/\Delta c$ for CIRs with local reverse shocks (S) or without (NS).

	P		$\Delta V/V$		$\Delta V/V/\Delta c$	
	S	NS	S	NS	S	NS
ρ	0.60	0.28	0.08	0.16	0.69	−0.14
p.100%	2.5	17.1	78.4	41.4	0.7	47.2

S – shock, NS – no shock

no reverse shocks. The correlation coefficient is close to zero. In turn, there is a strong correlation between ion intensity and the compression width for simple-stream CIR events with in-situ reverse shocks. This correlation is highly significant with a probability of less than 0.5% that the sample comes from the random population. For compound-stream CIRs the correlations are weak and not statistically significant.

2.5 Peak intensity and compression

To have a more detail insight into the events with the simple streams, Fig. 4 plots the 0.189 MeV/n He ion intensity vs. peak pressure (left panel), relative flow-speed change (middle panel) and relative flow-speed change per width of the compression region (right panel). The last parameter could be a good measure of the flow-speed spatial gradients inside the CIR. The upper panels show events with in-situ reverse shocks, the lower panels without shocks. Open symbols indicate data added after decomposition of the CIRs with compound streams. Figure 4 shows that the bulk of the events have peak pressure between 0.1 and 0.6 nPa and a relative flow-speed change between 30 and 50%. One can see that the events with in-situ reverse shocks show a clear dependence of the He peak intensity on the pressure peak and also on flow-speed change normalized by the thickness of the compression. More details can be found in Table 3 which shows correlation coefficient ρ for He ion peak intensity with different parameters. The events with shocks show significant (<5%) moderate correlation between He ion peak intensity and peak pressure. The correlation remains moderate ($\rho\sim$0.49) if the outlier point in the graph, which is the event with maximum peak pressure (see Fig. 4, upper left panel), is not included in the analysis. The events without in-situ reverse shocks have

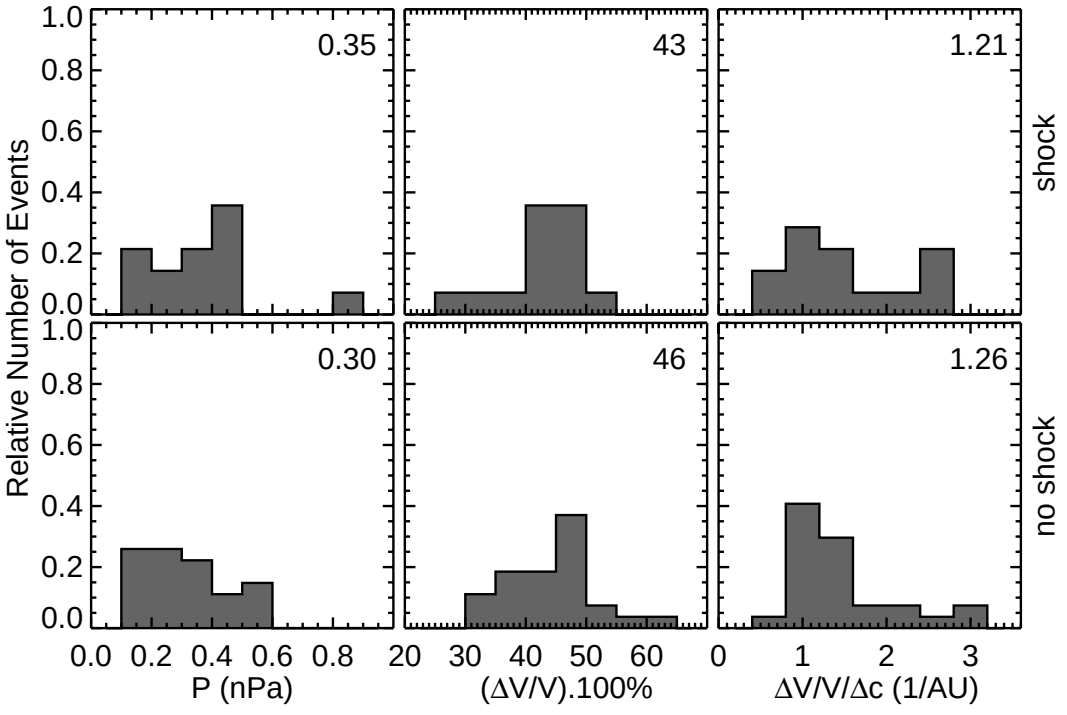

Fig. 5. Histograms of peak pressures (left), relative flow-speed changes (middle panel) and relative flow-speed changes per width of the compression region (right panel) for CIRs with simple streams. The medians are shown in the upper right corners.

only a weak correlation. In this group, there is also one outlier point – the event with highest intensity (event 05B) left out from the correlation. Although the online data for this CIR do not report on the reverse shock, the abrupt decrease in total pressure (see Fig. 2) may point to the developing reverse shock. The same CIR on spacecraft A, separated from S/C B in a half day of corotation, was accompanied by the shock. If event 05B is considered in the analysis, then the correlation coefficient weakly increase ($\rho \sim 0.35$). Table 3 shows that while there is no relationship between ion peak intensity and the relative flow-speed change for the events with local reverse shocks, the significant (<1%) strong correlation is found for the same parameter, normalized to the thickness of the compression region.

Figure 5 shows the distribution of the number of events by different parameters introduced in Fig. 4. The shape of the distributions in the left panels indicates that the non-shock group has more CIRs with smaller values of the peak pressure. The reverse situation is seen for CIRs with local shock. For example, only 36% of 14 CIRs with in-situ shock fall below 0.3 nPa, the median value of 27 non-shock CIRs. Shown in the middle panel, the relative change in the flow speed is roughly centrally distributed for non-shock CIRs. If the flow-speed change is normalized by the width of the compression region, then the CIRs without in-situ shocks have the peak of the distribution pushed to the left. Thus the bulk of the CIRs have lower spatial solar wind speed gradients. Note, the CIRs with in-situ shocks show similar distribution by solar wind speed gradients. The difference between medians is only 4%.

Finally, Fig. 6 shows the distribution of the number of CIRs (with simple streams and decomposed) by relative difference between the compression width and the model predicted maximum size of the compression region given by Eq. (2) in Giacalone et al. (2002). The CIRs with the negative difference have width below the model predicted maximum and according to the compressional theory the acceleration could occur. It is clearly seen that the bulk of the CIRs without in-situ reverse shock have compression width more than 30% higher than the maximum width. In case of CIRs bounded by the shock the asymmetry in the distribution is not so high.

3 Discussion

The presented observations show a strong negative correlation between the ion intensity and compression width for CIR events with in-situ reverse shocks. This leads to the question whether the scale of the region downstream of the reverse shock (i.e. inside the CIR) is a parameter that organizes the intensity of the shock accelerated ions in the CIR. If shock acceleration is what is going on, the thickness of the region should not play a role. We also found that the ion intensity

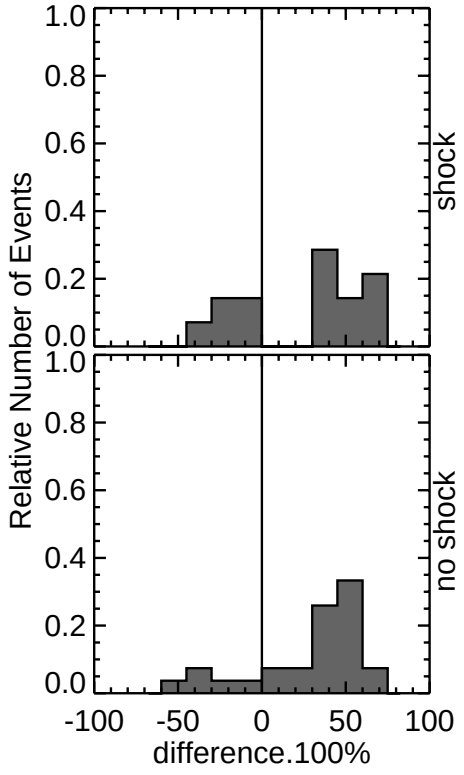

Fig. 6. Histograms of differences between the compression width and its theoretical maximum for CIRs with simple streams.

is positively correlated with pressure peak and with the flow-speed change per width of the compression. This additionally indicates that along with the shock the characteristics of the compression region may also determine the acceleration process. One way to interpret these correlations is that the particles are pre-accelerated inside the CIR by the compressional mechanism for further shock acceleration. The similar idea has been proposed by Schwadron et al. (1996) for the interstellar pick-up ion acceleration in CIRs. The authors suggest that particles first undergo statistical acceleration inside the CIR, reaching the speeds above the shock acceleration threshold, and then accelerated at forward and reverse shocks which surround the CIR.

However, no relationship between the intensity and compression width has been found for CIRs not bounded by reverse shocks. We suggest the following interpretation. We have shown that the majority of the events within this group have low spatial solar wind speed gradients and the peak pressure (see Fig. 5). This indicates that the compression is weak and therefore the acceleration could not operate. Richardson (2004) also noted that it is unclear whether such a process could operate in CIR with slight velocity gradient. In addition, the bulk of the CIRs have considerably larger compression width than the thickness allowed by the acceleration theory. The particles are likely to be accelerated by other mechanism, e.g. by the distant reverse shock. Connection to the shock and/or transport may result in the relatively low observed intensities. Since the region inside the CIR is not nominally connected to the distant reverse shock (e.g., Intriligator and Siscoe, 1994), and majority of the investigated events peaked within the CIR, additionally we require a mechanism which populates the field lines inside the compression region. Dwyer et al. (1997) provided observational evidence for perpendicular transport across magnetic field lines. We also cannot entirely exclude the uncertainty in the determination of the thickness of the compression region which could mimic the investigated relationship. Note, however, that 70% of the simple-stream CIRs with no in-situ reverse shocks were well defined, according to Table 1. Excluding from the analysis the events with unclear boundaries the correlation still remains zero. We also consider the peak of the total pressure as a more rigid parameter compared to the thickness of the compression zone. The relation between the ion intensity and the peak pressure still remains weak. In future studies we will look for signs of increased local turbulence as a possible contributing mechanism for the He in compression regions.

An alternative way of looking at these results is to consider that the events with shocks developed at 1 AU are cases where acceleration is going on nearby. Thus, the locally measured plasma pressures show a significant correlation with the particle peak intensity. For cases where the shock or acceleration is taking place beyond (perhaps well beyond) 1 AU, the correlation with the 1 AU plasma parameters would be expected to be weaker or non-existent. So the two sets of events being discussed may be those with acceleration close to 1 AU ("shocks") and those further away ("no shocks"), and then the correlation or lack of it follows.

Around one third of the CIRs during the investigated period were bounded by well-developed reverse shocks. It is similar to the 31% occurrence rate of shocks at CIRs at 1 AU during the period 1995–2004, as reported by Jian et al. (2006). Earlier observations reveal that few CIRs are bounded by shocks at 1 AU, but that most are at larger heliocentric distances (e.g., Hundhausen and Gosling, 1976). Jian et al. (2006) consider that the low quality of earlier data, combined with the variations from solar cycle to solar cycle may lead to the lower number of shocks found in the previous observations. These new observations suggest that the shock acceleration at energies below 1 MeV/n appears to be an important mechanism also at heliocentric distances around 1 AU. Figure 4 shows that only 8 CIRs were able to produce He ion intensity greater than 100 particles/cm^2 s sr MeV/n. From this number, 7 CIRs were accompanied by the reverse shocks. For the remaining event, which is the event 05B, we have already mentioned that the likely source of the high intensity could be a reverse shock. This also suggests that the shock mechanism is the only powerful source of the energetic ions in the CIR events. Moreover, there are other events, 04B, 16B, and 31B, where He ion intensity shows

a sharp peak at all energies accompanied by pressure jumps being consistent with reverse shock. Thus, possibly in 40% of the analyzed events the local reverse shock was the source of the ion enhancement.

4 Summary

We examined 50 CIR events between the February 2007 and September 2008 solar minimum period. The analysis of the 27 events without local shocks indicates that the data are not organized as expected if a compressional mechanism dominates. There is also an observed lack of dependence of ion intensity on the solar wind speed gradients and the peak pressure. We suggest that since the events we have analyzed have low solar wind speed gradients, low peak pressures and large widths, the compressional mechanism could not work. But for the 14 events with local reverse shocks, the particle intensity shows inverse dependence on the width of the compression region, consistent with the compressional acceleration model. A possible implication is that the characteristics of the compression region (like width of the scattering zone, solar wind speed gradients, and total pressure) in CIRs with fully developed shocks appear to be the parameter which may control the efficiency of the acceleration in the CIR events. We also conclude that the local shock acceleration at 1 AU appears to be an important ion source also at lower energies.

Acknowledgements. We thank J. G. Luhmann for suggestions concerning the CIRs boundaries and N. Gopalswamy for comments on the shock acceleration. We would also like to thank B. Podlipnik for his support in the computer and network areas. We acknowledge STEREO PLASTIC under NASA Contract NAS5-00132 for the use of solar wind plasma data. STEREO LET data were obtained from http://www.srl.caltech.edu. This work was supported by the Max-Planck-Gesellschaft zur Förderung der Wissenschaften and the Bundesministerium für Bildung und Forschung (BMBF) under grant 50 OC 0501. The work at the Johns Hopkins University/Applied Physics Laboratory was supported by NASA under contract SA4889-26309 from the University of California Berkeley.

The service charges for this open access publication have been covered by the Max Planck Society.

Topical Editor R. Forsyth thanks M. Popecki and another anonymous referee for their help in evaluating this paper.

References

Acuña, M. H., Curtis, D., Scheifele, J. L., Russell, C. T., Schroeder, P., Szabo, A., and Luhmann, J. G.: The STEREO/IMPACT Magnetic Field Experiment, Space Sci. Rev., 136, 203–226, 2008.

Barnes, C. W. and Simpson, J. A.: Evidence for interplanetary acceleration of nucleons in corotating interaction regions, Astrophys. J., 210, 91–96, 1976.

Belcher, J. W. and Davis Jr., L.: Large-amplitude Alfvén waves in the interplanetary medium, 2., J. Geophys. Res., 76, 3534–3563, 1971.

Bučík, R., Gómez-Herrero, R., Korth, A., Mall, U., and Mason, G. M.: Energetic ions from corotating interaction regions during small solar events in May 2007, in: Proceedings of the 21st European Cosmic Ray Symposium, Košice, Slovakia, 9–12 September 2008, 322–327, 2009.

Burlaga, L. F.: Interplanetary magnetohydrodynamics, Oxford University Press, New York, 1995.

Chotoo, K., Schwadron, N. A., Mason, G. M., Zurbuchen, T. H., Gloeckler, G., Posner, A., Fisk, L. A., Galvin, A. B., Hamilton, D. C., and Collier, M. R.: The suprathermal seed population for corotating interaction region ions at 1 AU deduced from composition and spectra of H^+, He^{++}, and He^+ observed on Wind, J. Geophys. Res., 105, 23107–23122, 2000.

Christon, S. P. and Simpson, J. A.: Separation of corotating nucleon fluxes from solar flare fluxes by radial gradients and nuclear composition, Astrophys. J., 227, 49–53, 1979.

Dwyer, J. R., Mason, G. M., Mazur, J. E., Jokipii, J. R., von Rosenvinge, T. T., and Lepping, R. P.: Perpendicular transport of low-energy corotating interaction region – associated nuclei, Astrophys. J., 490, 115–118, 1997.

Fisk, L. A. and Gloeckler, G.: The common spectrum for accelerated ions in the quiet-time solar wind, Astrophys. J., 640, 79–82, 2006.

Fisk, L. A. and Lee, M. A.: Shock acceleration of energetic particles in corotating interaction regions in the solar wind, Astrophys. J., 237, 620–626, 1980.

Galvin, A. B., Kistler, L. M., Popecki, M. A., et al.: The Plasma and Suprathermal Ion Composition (PLASTIC) investigation on the STEREO observatories, Space Sci. Rev., 136, 437–486, 2008.

Giacalone, J. and Jokipii, J. R.: Spatial variation of accelerated pickup ions at co-rotating interaction regions, Geophys. Res. Lett., 24, 1723–1726, 1997.

Giacalone, J., Jokipii, J. R., and Kóta, J.: Particle acceleration in solar wind compression regions, Astrophys. J., 573, 845–850, 2002.

Gómez-Herrero, R., Klassen, A., Müller-Mellin, R., Heber, B., Wimmer-Schweingruber, R., and Böttcher, S: Recurrent CIR-accelerated ions observed by STEREO SEPT, J. Geophys. Res., 114, A05101, doi:10.1029/2008JA013755, 2009.

Gosling, J. T. and Pizzo, V. J.: Formation and evolution of corotating interaction regions and their three dimensional structure, Space Sci. Rev., 89, 21–52, 1999.

Hundhausen, A. J. and Gosling, J. T.: Solar wind structure at large heliocentric distances – an interpretation of Pioneer 10 observations, J. Geophys. Res., 81, 1436–1440, 1976.

Intriligator, D. S. and Siscoe, G. L.: Stream interfaces and energetic ions closer than expected: Analyses of Pioneers 10 and 11 observations, Geophys. Res. Lett., 21, 1117–1120, 1994.

Jian, L., Russell, C. T., Luhmann, J. G., and Skoug, R. M.: Properties of stream interactions at one AU during 1995–2004, Solar Phys., 239, 337–392, 2006.

Kaiser, M. L., Kucera, T. A., Davila, J. M., St. Cyr, O. C., Guhathakurta, M., and Christian, E.: The STEREO mission: An introduction, Space Sci. Rev., 136, 5–16, 2008.

Kallenbach, R., Geiss, J., Gloeckler, G., and von Steiger, R.: Pick-up ion measurements in the heliosphere – a review, Astrophys.

Space Sci., 274, 97–114, 2000.

Klecker, B., Bogdanov, A. T., Galvin, A. T., Ipavich, F. M., Hilchenbach, M., Möbius. E., and Bochsler, P.: On the variability of suprathermal He^+ ions at 1 AU, in: Proceedings of ICRC 2001, 3100–3103, 2001.

Kocharov, L., Kovaltsov, G. A., Torsti, J., Anttila, A., and Sahla, T.: Modeling the propagation of solar energetic particles in corotating compression regions of solar wind, J. Geophys. Res., 108, 1404, doi:10.1029/2003JA009928, 2003.

Mason, G. M.: Composition and energy spectra of ions accelerated in corotating interaction regions, in: Acceleration and Transport of Energetic Particles Observed in the Heliosphere: ACE 2000 Symposium, AIP Conference Proc., 528, 234–241, 2000.

Mason, G. M., Mazur, J. E., Dwyer, J. R., Reames, D. V., and von Rosenvinge, T. T.: New spectral and abundance features of interplanetary heavy ions in corotating interaction regions, Astrophys. J., 486, 149–152, 1997.

Mason, G. M., von Steiger, R., Decker, R. B., et al.: Origin, injection, and acceleration of CIR particles: Observations, Space Sci. Rev., 89, 327–367, 1999.

Mason, G. M., Leske, R. A., Desai, M. I., Cohen, C. M. S., Dwyer, J. R., Mazur, J. E., Mewaldt, R. A., Gold, R. E., and Krimigis, S. M.: Abundances and energy spectra of corotating interaction region heavy ions observed during solar cycle 23, Astrophys. J., 678, 1458–1470, 2008a.

Mason, G. M., Korth, A., Walpole, P. H., Desai, M. I., von Rosenvinge, T. T., and Shuman, S. A.: The Suprathermal Ion Telescope (SIT) for the IMPACT/SEP investigation, Space Sci. Rev., 136, 257–284, 2008b.

Mason, G. M., Desai, M. I., Mall, U., Korth, A., Bucik, R., von Rosenvinge, T. T., and Simunac, K. D.: In situ observations of CIRs on STEREO, Wind, and ACE During 2007–2008, Solar Phys., 256, 393–408, 2009.

Mewaldt, R. A., Cohen, C. M. S., Cook, W. R., et al.: The Low-Energy Telescope (LET) and SEP central electronics for the STEREO mission, Space Sci. Rev., 136, 285–362, 2008.

Möbius, E., Hovestadt, D., Klecker, B., Scholer, M., Gloeckler, G., and Ipavich, F. M.: Direct observation of He^+ pick-up ions of interstellar origin in the solar wind, Nature, 318, 426–429, 1985.

Möbius, E., Morris, D., Popecki, M. A., Klecker, B., Kistler, L. M., and Galvin, A. B.: Charge states of energetic ($\approx$ 0.5 MeV/n) ions in corotating interaction regions at 1 AU and implications on source populations, Geophys. Res. Lett., 29, 1016, doi:10.1029/2001GL01 3410, 2002.

Richardson, I. G.: Low energy ions in co-rotating interaction regions at 1 AU: Evidence for statistical ion acceleration, Planet. Space Sci., 33, 557–569, 1985.

Richardson, I. G.: Energetic particles and corotating interaction regions in the solar wind, Space Sci. Rev., 111, 267–376, 2004.

Richardson, I. G. and Zwickl, R. D.: Low energy ions in corotating interaction regions at 1 AU: Observations, Planet. Space Sci., 32, 1179–1193, 1984.

Sanderson, T. R., Lin, R. P., Larson, D. E., et al.: Wind observations of the influence of the Sun's magnetic field on the interplanetary medium at 1 AU, J. Geophys. Res., 103, 17235–17247, 1998.

Schwadron, N. A., Fisk, L. A., and Gloeckler, G.: Statistical acceleration of interstellar pick-up ions in co-rotating interaction regions, Geophys. Res. Lett., 23, 2871–2874, 1996.

Siscoe, G. L.: Three-dimensional aspects of interplanetary shock waves, J. Geophys. Res., 81, 6235–6241, 1976.

Smith, E. J. and Wolfe, J. H.: Fields and plasmas in the outer solar system, Space Sci. Rev., 23, 217–252, 1979.

Zhang, M.: Theory of energetic particle transport in the magnetosphere: A noncanonical approach, J. Geophys. Res., 111, A04208, doi:10.1029/2005JA011323, 2006.